GMR
The Original

A BIO-INSPIRED SPIKING NEURAL NETWORK FOR AUTOMATED BRAIN TUMOR CLASSIFICATION USING MRI IMAGES

Divya S R[1], Bharathi M G[2], Sulakshana R K[3], Sandhya Malayanur[4]

[1] Selection Grade-Assistant Professor, Department of Computer Science, Vijaya College, RV Road, Basavanagudi, Bengaluru, Karnataka 560004, Email Id: srdivya7306@gmail.com
[2] Selection Grade-Assistant Professor, Department of Computer Science, Vijaya college, R V Road, Basavanagudi, Bengaluru, Karnataka 560004, Email Id: bharathimg@gmail.com
[3] Assistant Professor, Department of Computer Applications, Dayananda Sagar Business Academy, Udayapura, Kanakapura Main Rd, Bengaluru, Karnataka 560082, Email Id: sulakshana.narendra@gmail.com
[4] Assistant Professor, Department of Computer Applications, Jyothy Institute of Commerce and Management, Thathaguni, off Kanakapura road, Bengaluru Karnataka 560082, Email Id: sandhyamalayanur80@gmail.com

ABSTRACT:
Brain tumors are among the most serious neurological disorders and can pose a significant risk to human life if not diagnosed at an early stage. Magnetic Resonance Imaging (MRI) is widely used for brain tumor diagnosis because it provides detailed images of brain tissues. However, accurately classifying brain tumors from MRI images remains a challenging task due to variations in tumor size, shape, location, texture, and intensity. To overcome these challenges, this study presents a machine learning-based approach for brain tumor classification using a Spiking Neural Network (SNN). Inspired by the functioning of biological neurons, SNNs effectively learn complex patterns from medical images while offering improved computational efficiency. In the proposed approach, MRI images are first segmented using Sharp No New U-Net (SnnU-Net), which accurately identifies tumor regions with different shapes and intensity levels. Next, texture, shape, and intensity features are extracted to capture the distinctive characteristics of tumor tissues. These features are then used to train the Spiking Neural Network for accurate brain tumor classification. The proposed method is evaluated using the BraTS2019, BraTS2020, and BraTS2021 benchmark datasets, achieving classification accuracies of 99.67%, 99.89%, and 99.93%, respectively. The experimental results demonstrate that the proposed SNN-based machine learning model provides highly accurate and reliable brain tumor classification, outperforming conventional neural network-based approaches and showing strong potential for supporting computer-aided diagnosis in clinical practice.

KEYWORDS: Brain tumor classification, Magnetic Resonance Imaging (MRI), Spiking Neural Network (SNN), Sharp No New U-Net (SnnU-Net);

1. INTRODUCTION

Brain tumors are among the most critical neurological disorders and can pose a serious threat to human life if they are not detected and treated at an early stage. Consequently, brain tumor classification has become an important research area in medical image analysis. However, accurate classification of brain tumors from Magnetic Resonance Imaging (MRI) images remains challenging because of significant variations in tumor size, shape, location, texture, and intensity, which reduce the performance of automated classification systems. To address these challenges, this study proposes a machine learning-based brain tumor classification framework using a Spiking Neural Network (SNN). The framework employs Sharp No New U-Net (SnnU-Net) to accurately segment tumor regions from MRI images, followed by the extraction of texture-, shape-, and intensity-based features for effective tumor characterization. These discriminative features are then classified using the Spiking Neural Network, resulting in improved classification accuracy and computational efficiency. The proposed model achieves classification accuracies of 99.67%, 99.89%, and 99.93% on the BraTS2019, BraTS2020, and BraTS2021 datasets, respectively, outperforming conventional Convolutional Neural Network (CNN)-based methods.
The human brain is one of the most complex and vital organs, consisting of billions of interconnected neurons, synapses, and nerve cells that regulate numerous physiological functions, but it is also susceptible to abnormalities such as brain tumors [1]. Medical image classification has become an essential component of biomedical research; however, developing reliable and accurate classification methods remains a significant challenge despite numerous advances [2]. Brain tumors are commonly classified based on histopathological characteristics and molecular biomarkers, which help determine the tumor type and grade for predicting disease progression, selecting appropriate treatment strategies, and identifying suitable candidates for clinical trials [3].
According to Global Cancer Statistics, tumors affecting the brain and nervous system are among the leading causes of cancer-related mortality worldwide [4]. Computed Tomography (CT) and Magnetic Resonance Imaging (MRI) are the primary imaging modalities used for brain tumor diagnosis, with MRI being the preferred technique because of its excellent soft-tissue contrast and ability to provide detailed anatomical information for assessing tumor size, location, and

type [5–7]. In addition, MRI enables continuous monitoring of disease progression and treatment response, making it an indispensable imaging modality in clinical practice [5]. Early detection of brain tumors through MRI-based image analysis significantly improves treatment planning and helps prevent further tumor progression [8].

Brain tumors exhibit substantial variations in morphology and appearance, ranging from benign to highly malignant lesions, making accurate diagnosis a challenging task [9]. Since treatment decisions depend on the tumor type, grade, and stage, timely and precise diagnosis plays a crucial role in improving patient outcomes [10]. Although manual segmentation of MRI images by radiologists remains the clinical standard, it is labor-intensive, time-consuming, and unsuitable for large-scale datasets, thereby necessitating the development of automated tumor segmentation techniques [11].

Recent advances in deep learning have significantly improved medical image analysis. Convolutional Neural Networks (CNNs) have demonstrated superior performance in feature extraction, segmentation, and classification compared with conventional image processing methods [12]. Similarly, Long Short-Term Memory (LSTM) networks have been explored for modeling sequential information in brain MRI analysis [13]. Nevertheless, accurate brain tumor classification remains challenging because of the complexity of tumor morphology, limited availability of annotated medical datasets, and the high computational cost of training robust deep learning models [14,15]. Furthermore, conventional data augmentation techniques, such as image rotation and flipping, are often insufficient for capturing the complex anatomical variations present in brain MRI images [16].

To overcome these limitations, this research presents a machine learning-based brain tumor classification framework using a Spiking Neural Network (SNN). Inspired by the biological behavior of neurons, SNNs process information through discrete spikes, enabling efficient learning while reducing computational complexity. Combined with accurate tumor segmentation and comprehensive feature extraction, the proposed framework provides reliable and efficient brain tumor classification from MRI images.

The major contributions of this research are summarized as follows:

- A machine learning-based brain tumor classification framework using a Spiking Neural Network (SNN) is proposed to efficiently classify MRI images by learning discriminative tumor characteristics while reducing computational complexity and improving classification performance.
- Sharp No New U-Net (SnnU-Net) is employed for accurate tumor segmentation. Its sharpness-aware loss function improves boundary localization, while hierarchical feature extraction and skip connections enhance the segmentation of tumors with complex shapes and varying intensity distributions.
- Multiple complementary feature extraction techniques, including Discrete Wavelet Transform (DWT), Local Ternary Pattern (LTP), Histogram of Oriented Gradients (HOG), Gray Level Co-occurrence Matrix (GLCM), histogram features, statistical features (mean, standard deviation, skewness, and kurtosis), and shape features, are integrated to capture texture, spatial, and intensity information, thereby improving the discriminative capability of the classification model.

The remainder of this paper is organized as follows. Section 2 reviews the related literature, Section 3 describes the proposed methodology, Section 4 presents the experimental results and discussion, and Section 5 concludes the paper.

2. PROPOSED METHODOLOGY

The proposed brain tumor classification framework uses MRI images obtained from the BraTS2019, BraTS2020, and BraTS2021 benchmark datasets. Initially, the MRI images undergo preprocessing, which includes image resizing and intensity normalization to ensure consistency in image dimensions and contrast across the datasets. These preprocessing steps improve the quality of the input data and enhance the performance of the subsequent analysis.

After preprocessing, the tumor regions are accurately segmented using Sharp No New U-Net (SnnU-Net), an enhanced version of the standard nnU-Net. The incorporation of a sharpness-aware loss function enables SnnU-Net to produce more precise tumor boundaries, even in MRI images with complex tumor shapes and varying intensity distributions.

Once the tumor regions are segmented, multiple complementary features are extracted to comprehensively characterize the tumor. These include texture features obtained using the Local Ternary Pattern (LTP) and Gray Level Co-occurrence Matrix (GLCM), frequency-domain features extracted through the Discrete Wavelet Transform (DWT), edge and gradient information captured using the Histogram of Oriented Gradients (HOG), statistical features such as mean, standard deviation, skewness, and kurtosis, histogram-based features, and shape descriptors. The integration of these diverse features provides a rich and discriminative representation of the tumor, improving the model's ability to distinguish between different tumor characteristics.

Finally, the extracted feature set is classified using a Spiking Neural Network (SNN), a biologically inspired machine learning algorithm that processes information through discrete spikes. The SNN effectively learns complex patterns from high-dimensional MRI data while maintaining computational efficiency, resulting in accurate and reliable brain tumor classification.

Figure 1 illustrates the overall workflow of the proposed brain tumor classification framework.

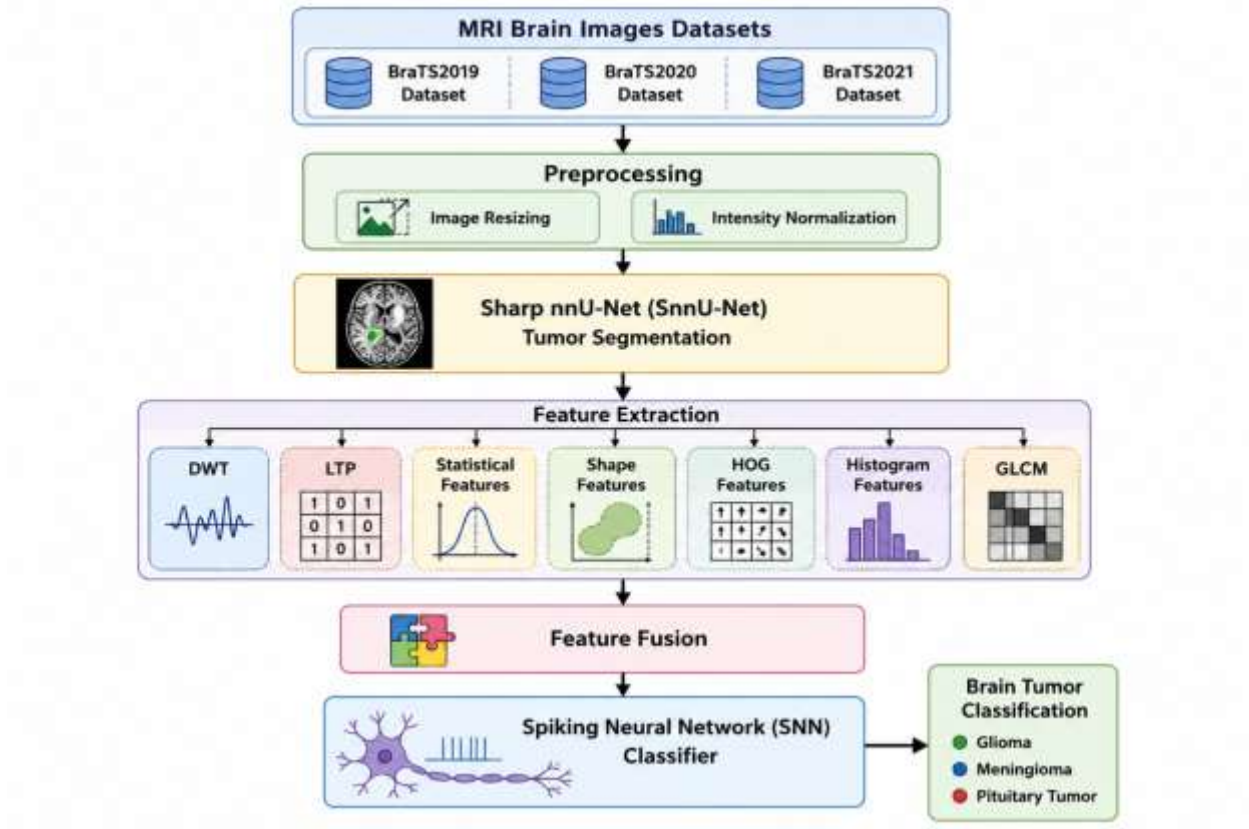

Figure 1. Overall process of Brain Tumor Classification

2.1 Dataset

In this study, brain tumor MRI images are obtained from three publicly available benchmark datasets: BraTS2019 [22], BraTS2020 [23], and BraTS2021 [24]. These datasets are widely used for developing and evaluating automated brain tumor analysis methods because they provide high-quality, expert-annotated MRI scans.

The BraTS2019 dataset consists of multi-institutional preoperative MRI scans of patients with Glioblastoma Multiforme (GBM)/High-Grade Glioma (HGG) and Low-Grade Glioma (LGG). It includes manually annotated ground-truth segmentation labels that are commonly used for training and validating brain tumor classification and segmentation models.

The BraTS2020 dataset extends the previous release by incorporating additional patient data and introducing more challenging cases, thereby improving the diversity and robustness of the benchmark dataset. It also supports research on clinically relevant tasks, such as patient survival prediction and tumor recurrence analysis.

The BraTS2021 dataset further enhances the benchmark by including a larger collection of clinically acquired multi-parametric MRI (mpMRI) scans of glioma patients. In addition to imaging data, it provides valuable clinical information, including pathological diagnoses and MGMT promoter methylation status, enabling the development of more comprehensive and clinically applicable machine learning models.

The combined use of the BraTS2019, BraTS2020, and BraTS2021 datasets provides a diverse set of MRI images that capture the heterogeneity of brain tumors, thereby improving the robustness and generalization capability of the proposed classification model. The distribution of the datasets is summarized in Table 1, while representative MRI images from each dataset are presented in Figure 2.

Table 1. Summary of data distribution

Datasets	Training samples	Validation samples	Total samples
BraTS2019	335	291	626
BraTS2020	369	291	660
BraTS2021	1032	219	1251

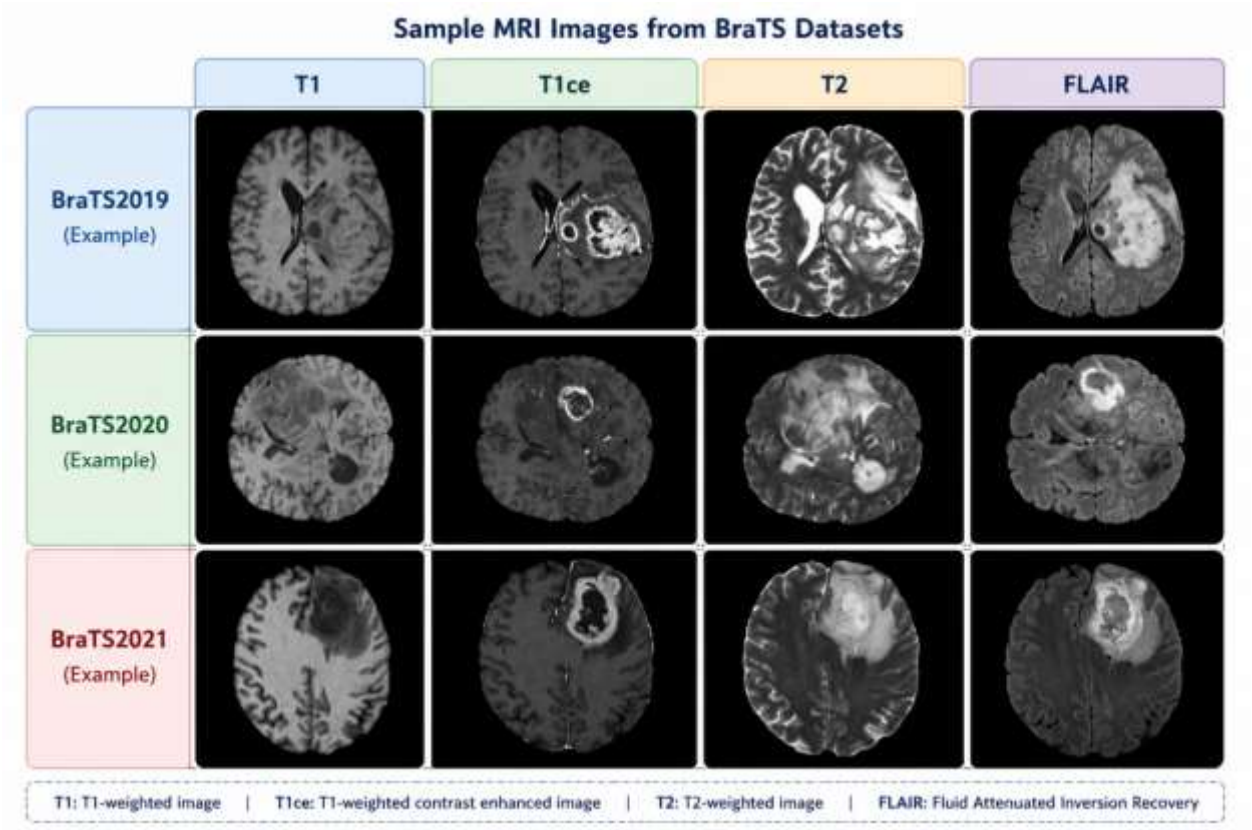

Figure 2. Sample images for BraTS2019, BraTS2020 and BraTS2021 datasets

2.2 Preprocessing

The preprocessing stage plays a vital role in improving the quality and consistency of MRI images before further analysis. Initially, all input MRI images are resized [9] to a standard resolution of 224 × 224 pixels to ensure uniform image dimensions across the entire dataset. Standardizing the image size eliminates dimensional inconsistencies, reduces computational complexity, and enables efficient training of the classification model. Moreover, it prevents biases caused by varying image resolutions and improves the model's ability to generalize across different MRI datasets.

Following the resizing step, intensity normalization [9] is performed to standardize the pixel intensity values of the MRI images. This process minimizes variations in image brightness and contrast that may arise due to differences in imaging equipment, acquisition protocols, or patient-specific characteristics. As a result, the classification model focuses on the intrinsic anatomical and pathological features of the brain rather than irrelevant intensity variations. Intensity normalization is particularly important in medical image analysis because it improves the consistency of the input data and enhances the robustness of the subsequent segmentation and classification stages. The mathematical expression used for intensity normalization is presented in Equation (1).

$$I_{norm}(i,j) = \frac{I(i,j) - I_{min}}{I_{max} - I_{min}} \qquad (1)$$

Through the normalization described in equation (1) pixel intensities receive specified range constraints which reduce illumination disparities to support effective learning of discriminative features by the model.

2.3 Segmentation

The proposed improved nnU-Net architecture is derived from the conventional U-Net framework, preserving its characteristic U-shaped encoder–decoder architecture while incorporating several architectural enhancements. In this study, the baseline nnU-Net framework is modified by increasing the network depth and expanding the number of convolutional filters in the encoder to improve feature extraction capability. Furthermore, an asymmetric network design is introduced to effectively handle multi-label segmentation tasks, thereby enhancing the model's representational capacity and learning efficiency.

The proposed architecture consists of a five-stage downsampling pathway, where each stage comprises two successive convolutional layers. During the first three downsampling stages, the number of feature channels is doubled after each stage, significantly increasing the model capacity and enabling the extraction of rich hierarchical features. Skip connections are employed to transfer high-resolution feature information from the encoder to the corresponding decoder stages, preserving spatial details and facilitating accurate feature reconstruction. In addition, a deep supervision strategy

is incorporated by integrating feature maps from multiple resolutions into the loss function, which improves gradient propagation, accelerates network convergence, and enhances overall segmentation accuracy.

The proposed Sharpness-aware nnU-Net (SnnU-Net) extends the conventional nnU-Net by introducing a sharpness-aware loss function to overcome the boundary smoothing limitations commonly encountered in medical image segmentation. Unlike conventional loss functions that primarily optimize regional overlap, the proposed sharpness-aware loss explicitly penalizes boundary prediction errors, resulting in improved edge preservation and more accurate delineation of tumor margins in brain MRI images.

Let A denote the set of all pixels in the MRI image, and let Md⊂ A represent the subset of pixels corresponding to potential boundary regions. The ground-truth segmentation and the predicted segmentation within the high-gradient boundary regions are denoted by ŷ and ŷ′, respectively, as defined in Equations (2) and (3). The sharpness-aware loss is formulated based on these components to enhance boundary localization while simultaneously preserving the overall segmentation accuracy.

$$\hat{y} = M_d \odot y \tag{2}$$

$$\hat{y}' = M_d \odot y' \tag{3}$$

$$L_{loss}(y_1, y_2) = \sum_{j=1}^{dn} \alpha_j [L_{dice}(y_1, y_2) + \omega * L_{CE}(y_1, y_2)] \tag{4}$$

$$L_{Global} = L_{loss}(y, y') \tag{5}$$

$$L_{Sharp} = L_{loss}(\hat{y}, \hat{y}') \tag{6}$$

The equations include segmentation outcomes representing ground truth y1 and y2 in loss function Lloss representing predictions. The total loss unites global and sharpness-aware components so the network becomes capable of learning both regional along with boundary-level information. The Dice term and Cross Entropy term constitute the formal Loss definitions as equation (7) and (8). Where, aj denotes the weight based on deep supervision modules as equation (9).

$$L_{Dice}(y, y') = -\frac{2\sum_{i=1}^{N}(y_i * y_i')}{\sum_{i=1}^{N} y_i + \sum_{i=1}^{N} y_i'} \tag{7}$$

$$L_{CE}(y, y') = -\frac{1}{N}\sum_{i=1}^{N}[y_i \log(y_i') + (1 - y_i)\log(1 - y_i')] \tag{8}$$

$$a_j = \frac{1}{\left[\sum_{j=1}^{dn} 1/2^{(j-1)}\right] 2^{(j-1)}} \tag{9}$$

The decoder pathway progressively reconstructs high-resolution feature maps, with the final segmentation output generated using a Sigmoid activation function. The resulting probability maps serve as inputs for both the global loss and the proposed sharpness-aware loss functions during network optimization. Each upsampling stage is designed to effectively propagate gradients throughout the network, facilitating stable training and improving the learning of fine structural details, particularly along object boundaries. By integrating multi-scale feature reconstruction with the sharpness-aware loss, the proposed SnnU-Net achieves superior segmentation performance, enabling more precise delineation of tumor boundaries and enhanced localization of brain tumors in MRI images.

2.4 Feature Extraction

Feature extraction is performed on the pre-processed MRI images to derive informative representations that facilitate accurate brain tumor segmentation. This stage plays a crucial role in reducing the dimensionality of large datasets by eliminating redundant and irrelevant information while preserving the most discriminative features. Consequently, the computational complexity of subsequent processing stages is reduced, leading to improved efficiency and segmentation performance. The extracted feature set comprises texture, shape, and intensity-based characteristics [25], which effectively capture the structural and anatomical properties of brain tissues, thereby enabling accurate tissue discrimination and robust feature representation for brain tumor analysis.

2.4.1 Discrete Wavelet Transform (DWT)

The Discrete Wavelet Transform (DWT) is employed to perform multiresolution analysis of MRI images, providing an effective framework for texture characterization and image representation. By decomposing the image into multiple frequency sub-bands, DWT captures both spatial and frequency-domain information at different resolution levels. The resulting feature vector incorporates complementary structural and textural characteristics, enabling comprehensive

representation of image content. Furthermore, DWT effectively preserves tissue texture, shape, and intensity information, thereby improving the detection of abnormal regions and facilitating accurate characterization of tissue properties.

2.4.2 Statistical Features

The quantitative measures from image analysis constitute statistical features. The pre-processed images generate statistical results including Mean values together with Standard Deviation (SD) data along with Skewness and Kurtosis outcomes in this research. The classification process benefits from these descriptors which analyze intensity distributions and variability patterns of brain tissues. The Statistical Features (SF) are concatenated and given in equation (10),

SF={Mean, SD, Skewness,Kurtosis} (10)

2.4.3 Shape and HOG Features

The extracted shape features provide a compact yet informative representation of the geometric and boundary characteristics of brain structures while reducing feature dimensionality. Descriptors such as area, perimeter, eccentricity, and solidity are computed to capture the morphological properties of the segmented regions. In addition, the Histogram of Oriented Gradients (HOG) is employed to characterize local shape information by encoding the orientation and magnitude of image gradients. These gradient-based features effectively emphasize edges and contours, thereby enhancing the discrimination of anatomical structures and improving the identification of brain tissue patterns.

2.4.4 Histogram Features

Histogram-based features describe the statistical distribution of pixel intensity values across the entire image and provide valuable information regarding tissue characteristics. In a histogram representation, the x-axis corresponds to pixel intensity levels, while the y-axis indicates the frequency of occurrence of each intensity value. These statistical descriptors effectively summarize the intensity distribution within the image, facilitating the differentiation of normal and abnormal tissues. Consequently, histogram-based features contribute to improved tissue characterization and support the accurate detection of pathological regions in brain MRI images.

2.4.5 Gray-Level Co-occurrence Matrix (GLCM)

The Gray-Level Co-occurrence Matrix (GLCM) is employed to extract second-order statistical texture features by analyzing the spatial relationships between pairs of pixels with specific gray-level intensities at predefined distances and angular orientations. This approach provides a quantitative characterization of image texture by capturing properties such as contrast, homogeneity, correlation, energy, and entropy, thereby enabling effective discrimination of tissue patterns in brain MRI images.

The final feature vector is constructed by concatenating the features extracted using the Discrete Wavelet Transform (DWT), Local Ternary Pattern (LTP), Statistical Features (SF), Shape Features, Histogram of Oriented Gradients (HOG), Histogram Features, and Gray-Level Co-occurrence Matrix (GLCM). The resulting unified feature representation is mathematically expressed in Equation (11).

X={DWT, LTP, SF, Shape, Hog, Histogram, GLCM} (11)

The resultant concatenated feature vector is the input for the next stage of brain tumor classification.

2.5 Classification

SNN provide an improved biological neural system because they use temporal information to model their neural computational structures. Revolutionary about SNN compared to artificial neural networks is their use of discrete binary spikes which the LIF controls. The LIF model serves as a widely used choice because of its basic design and efficient execution which simulates biological neuron activities through membrane potential integration and leakage to reach firing thresholds. The network implements scalar weights as artificial synapses to build its neural connections which resemble biological synapses. This research uses the LIF model because it provides the simplest approach to model pulsatile neuron potential dynamics and stands as the primary model selection for this purpose. Differential equations applied to the Hodgkin-Huxley model depict biological neuronal function more precisely because they include automated simulation of complicated ion channel behavior. Despite its mathematical complexity and reduced interpretability, the LIF model stands superior to the Hodgkin-Huxley model because it demonstrates analytical simplicity but maintains good alignment with empirical data. This allows it to find practical usage between computational efficiency and biological realism. The spiking neuron stands as the base computational element in SNN. A unified spiking model describes neuron type behaviors using a set of equation groups which are presented in equation (12)- (14),

$$H[t] = f(V[t-1], X[t]) \quad (12)$$

$$S[t] = \Theta(H[t] - V_{th}) \quad (13)$$

$$V[t] = H[t](1 - S[t]) + V_{reset}S[t] \quad (14)$$

Where, H[t] is a current input at particular time t, while H[t] and V[t] are membrane potential following neuronal activation and after trigger spike at time t correspondingly. The parameter V denotes firing threshold which Θ(x) represents the Heaviside function which creates binary nature of spike generation as equation (15),

Θx=1 for x=0 and Θx=0 for x<0 (15)

This function is defined such that Θx=1 when x is higher than or equal to 0 and Θx=0 when x is lesser than 0. This captures the fundamental approach through membrane potential and trigger approach relationship in SNN. The St denotes the peak output at specific time t which adopts the score of 1 when spike occurs otherwise 0 thereby denoting the reset potential This binary indicator score captures whether a neuron has fired or not at that given time. The function f is a spiking neuron

behavior is captured through the function while establishing various expressions based on modeling techniques. The function f represents different models as it takes from equation (16) and (17) in LIF. Each formulation includes specific firing behaviors and input stimulus responses which match the behavior of its represented model.

$$H[t] = V[t-1], X[t] \tag{16}$$

$$H[t] = V[t-1] + \frac{1}{\tau} X[t] - (V[t-1] - V_{rest}) \tag{17}$$

In this context π denotes membrane time constant which regulates how potential at membranes changes with time throughout neural dynamics. The basic spiking processes for spike generation and reset actions are described in equations (13) and (14) through shared by multiple spiking neuron models.

The proposed approach uses zero weighting for pruned synapses which happens during all phases including training and inference. Such synapses become irrelevant for both signal transmission and weight update processes during backpropagation or inference because they receive zero weight and lose their network influence. Let consider the jth neuron in hidden layer. xi is an input to neuron hj in hidden layer, yi is an output neuron hj, the wij and bj are weight and bias respectively. If Pw denotes a set of pruned synapses, then feedforward and feedback function is specified in equation (18)- (20),

$$y_i = f\left(\sum_{i=1}^{n} p(w_{ij}) w_{ij} x_i + b_j\right) \tag{18}$$

$$w_{ij} = p(w_{ij}) \times \left(w_{ij} - \eta \frac{\partial E}{\partial w_{ij}}\right) \tag{19}$$

$$p(w_{ij}) = \begin{cases} 1, & w_{ij} \notin P_w \\ 0, & w_{ij} \notin P_w \end{cases} \tag{20}$$

Where, f is activation function, E is loss function and η is learning rate. If the synapse is a part of pruned synapse set Pw, it will not excluded from both used and updated. The computation through temporal spike-based information transfer in CPSNN leads to efficient medical data processing especially when dealing with high-dimensional data sets such as MRI scans. The cognitive pruning mechanism decreases the computational complexity while reducing memory usage while yielding equivalent accuracy levels. The model achieves faster inference because of pruning which makes real-time deployment possible for clinical use. The biologically inspired CPSNN structure helps it detect hidden spatial and temporal patterns in tumor regions effectively.

3. RESULT ANALYSIS

The SNN is simulated in Python with system configuration of Windows 10 OS, RAM 16GB and intel i5 processor. The Dice Score Coefficient (DSC), Intersection over Union (IoU) and Hausdorff Distance (HD) are considered for analyzing the segmentation performance. Furthermore, the accuracy, F1-score, precision and sensitivity are considered for analyzing the classification performance. The mathematical presentation for these metrics is explained in equation (21)- (27).

$$DSC = \frac{2TP}{2TP + FP + FN} \tag{21}$$

$$IoU = \frac{TP}{(TP + FP + FN)} \tag{22}$$

$$HD(X,Y) = max\left\{\max_{x \in X} \min_{y \in Y} \|x - y\|, \max_{y \in Y} \min_{x \in X} \|y - x\|\right\} \tag{23}$$

$$Accuracy = \frac{TP + TN}{TP + TN + FP + FN} \tag{24}$$

$$F1 - score = 2 \times \frac{Precision \times Sensitivity}{Precision + Sensitivity} \tag{25}$$

$$Precision = \frac{TP}{TP + FP} \tag{26}$$

$$Sensitivity = \frac{TP}{TP + FN} \tag{27}$$

Where, TP, FP, TN and FN denotes True Positive, False Positive, True Negative and False Negative respectively. The X and Y are two point sets, x−y is Euclidean distance between point x in set X and point y in set Y. The max and min are minimum and maximum values in a set of numbers.

3.1 Performance Analysis

The performance of SnnU-Net model is described for BraTS2019, BraTS2020 and BraTS2021 dataset with metrics of DSC, IoU and HD as Table 2. The U-Net, Residual U-Net (ResU-Net) and nnU-Net performances are taken and compared with SnnU-Net model. The SnnU-Net model achieves better performance of 98.26% DSC, 97.85% IoU and 10.47% HD on BraTS2019 dataset. For BraTS2020 dataset, it achieves 98.12% DSC, 98.67% IoU and 8.33% HD. Moreover, it achieves 99.54% DSC, 98.96% IoU, and 7.29 HD for BraTS2021 dataset.

Table 2. Performance of SnnU-Net with different segmentation models

Dataset	Methods	DSC (%)	IoU (%)	HD (%)
BraTS2019	U-Net	93.82	92.45	15.62
	ResU-Net	95.73	94.34	13.48
	nnU-Net	96.45	95.67	12.08
	SnnU-Net	98.26	97.85	10.47
BraTS2020	U-Net	94.34	92.87	14.45
	ResU-Net	96.23	95.01	12.72
	nnU-Net	97.56	96.34	10.92
	SnnU-Net	99.12	98.67	8.33
BraTS2021	U-Net	94.96	93.18	13.81
	ResU-Net	96.85	95.12	11.76
	nnU-Net	98.02	96.87	9.92
	SnnU-Net	99.54	98.96	7.29

The SnnU-Net delivers superior brain tumor segmentation results than U-Net, ResU-Net, and nnU-Net through its framework which promotes exact boundary finding and hierarchical feature extraction capabilities. The design of this model includes optimized skip connections together with advanced upsample processes that lead to better identification of tumor regions particularly within edges and small features. An efficient framework yields better measurements in both DSC and IoU metrics which demonstrate improved overlap with reference data. At the same time, it produces reduced HD scores that show better spatial matching. SnnU-Net surpasses BraTS dataset results because it expands nnU-Net adaptive capabilities with additional enhancements that preserve detailed information.

The performance of SNN is described for BraTS2019, BraTS2020 and BraTS2021 dataset with metrics of accuracy, F1-score, precision and sensitivity as Table 3. The Artificial Neural Network (ANN), CNN and SNN performances are taken and compared with CPSNN. The CPSNN achieves better performance of 99.67% accuracy, 99.15% F1-score, 99.24% precision and 99.16% sensitivity on BraTS2019 dataset. Additionally, it achieves 99.89% accuracy, 99.16% F1-score, 99.37% precision and 99.22% sensitivity on BraTS2020 dataset. For BraTS2021 dataset, it achieves 99.93% accuracy, 99.26% F1-score, 99.57% precision and 99.34% sensitivity for BraTS2021 dataset.

Table 3. Performance of proposed SNN with different classification models

Dataset	Methods	Accuracy (%)	F1-score (%)	Precision (%)	Sensitivity (%)
BraTS2019	ANN	95.23	94.58	94.10	94.34
	CNN	96.45	95.67	95.22	95.44
	SNN	97.51	96.78	96.12	96.45
	CPSNN	99.67	99.15	99.24	99.16
BraTS2020	ANN	95.67	94.92	94.36	94.64
	CNN	96.80	96.02	95.40	95.71
	SNN	97.85	97.21	96.55	96.88
	CPSNN	99.89	99.16	99.37	99.22
BraTS2021	ANN	96.12	95.45	94.88	95.16
	CNN	97.20	96.43	95.80	96.11
	SNN	98.31	97.55	96.94	97.24
	CPSNN	99.93	99.26	99.57	99.34

SNN demonstrates better brain tumor classification capability than ANN, CNN and SNN since its event-driven calculation and dynamic synaptic pruning mechanism duplicates how the brain conducts efficient information processing. The neural network architecture of SNN differs from ANN and CNN since its biologically inspired spiking neurons together with adaptive pruning mechanism helps remove unnecessary connections to decrease processing noise while maintaining better accuracy. The implementation produces enhanced generalization with minimal computational expenses. The time-based representation of SNN enables precise identification of detailed MRI patterns which enhances precise tumor boundary identification. Through pruning, the network becomes more efficient by preventing overfitting while keeping essential paths active for making decisions.

The complexity analysis of SNN is provided in Table 4 in terms of execution time and memory usage for BraTS2019, BraTS2020 and BraTS2021 datasets. The ANN, CNN and SNN complexity are compared with SNN for all three datasets. The SNN achieves less execution time of 15.7s, 14.2s and 13.5s for BraTS2019, BraTS2020 and BraTS2021 datasets respectively. Similarly, it achieves memory usage of 8.2MB, 7.5MB and 5.9MB for BraTS2019, BraTS2020 and BraTS2021 datasets correspondingly.

Table 4. Complexity analysis for different classification models

Dataset	Methods	Execution time (s)	Memory Usage (MB)
BraTS2019	ANN	20.2	12.5
	CNN	19.5	10.7
	SNN	17.4	9.8
	SNN	15.7	8.2
BraTS2020	ANN	19.6	12.7
	CNN	17.8	11.1
	SNN	16.9	9.3
	SNN	14.2	7.5
BraTS2021	ANN	18.5	9.1
	CNN	16.1	8.3
	SNN	14.7	6.7
	SNN	13.5	5.9

The confusion matrix for BraTS2019, BraTS2020 and BraTS2021 datasets are given in Figure 3 which illustrates classification performance among all four MRI modalities such as T1, T1Gd, T2 and T2-FLAIR. Every matrix illustrates a better diagonal dominance which indicates better accuracy in predicted labels closely matches the true labels. The nominal off-diagonal values replicate fewer misclassification which denotes the model effectively differentiate among various MRI sequences. This performance among various datasets such as BraTS2019, BraTS2020 and BraTS2021 provides generalizability and robustness of the model.

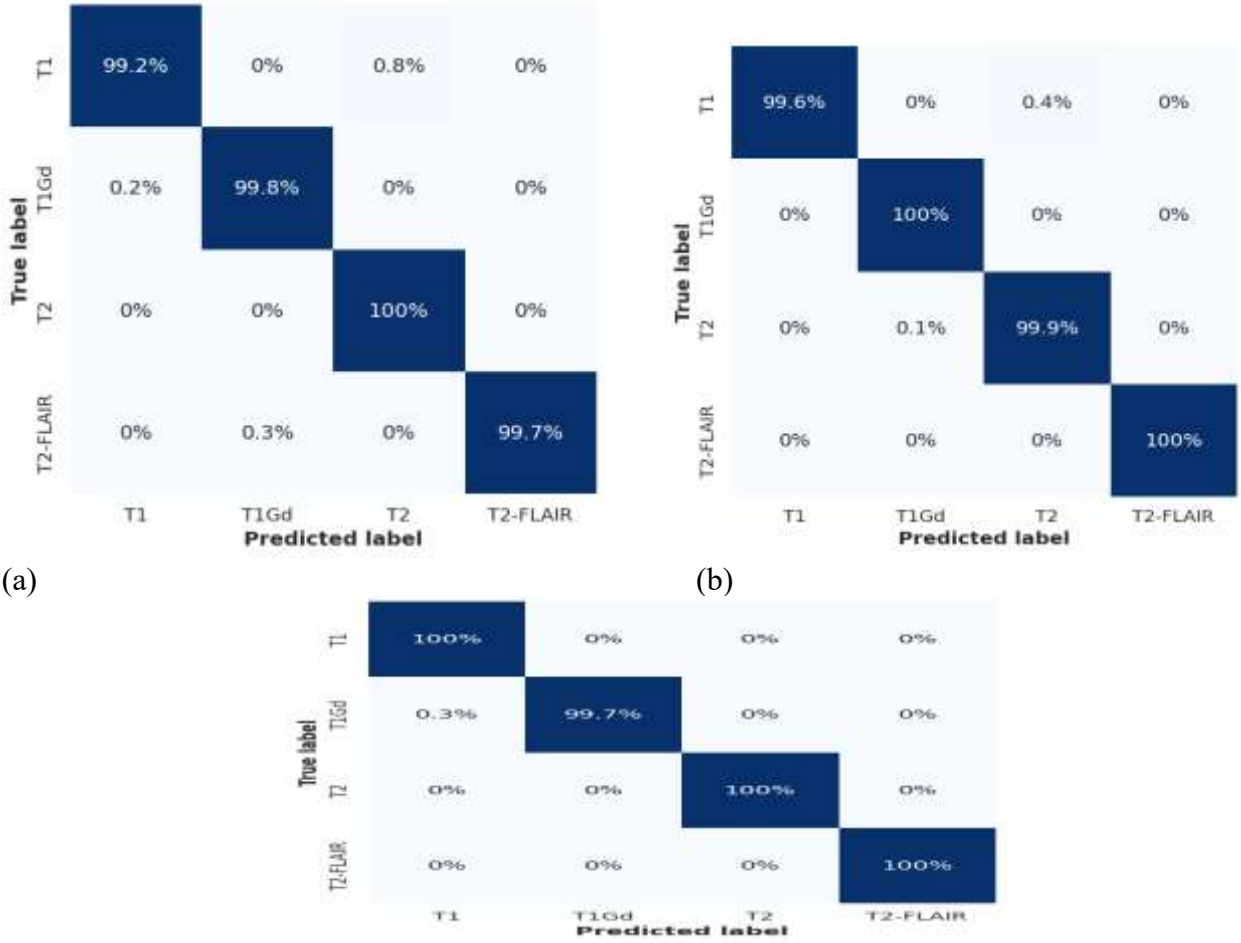

Figure 3. Confusion matrix (a) BraTS2019, (b) BraTS2020 and (c) BraTS2021 dataset

3.2 Comparative Analysis

The performance comparison of the proposed SNN with existing methods on the BraTS2019, BraTS2020, and BraTS2021 datasets is presented in Table 4. The evaluation is performed using accuracy, F1-score, precision, and sensitivity metrics. The compared methods include CNN-based Bayesian Optimized SVM [17], Relevance Score with AWA-based VGG-19 [18], IGANN HBD-MI [19], CNN [20], and ARM-Net [21].

The proposed SNN achieves superior performance across all datasets, obtaining 99.67% accuracy, 99.15% F1-score, 99.24% precision, and 99.16% sensitivity on BraTS2019. For BraTS2020, it achieves 99.89% accuracy, 99.16% F1-score, 99.37% precision, and 99.22% sensitivity, while BraTS2021 results show 99.93% accuracy, 99.26% F1-score, 99.57% precision, and 99.34% sensitivity. These results confirm the effectiveness of CPSNN in achieving accurate and robust brain tumor classification.

Table 4. Comparative analysis with existing methods for all three datasets

Dataset	Method	Accuracy (%)	F1-score (%)	Precision (%)	Sensitivity (%)
BraTS2019	Relevance score with the AWA-based VGG-19 [18]	96.20	NA	NA	NA
	CNN [20]	99.55	98	98	98
	SNN	99.67	99.15	99.24	99.16
BraTS2020	Relevance score with the AWA-based VGG-19 [18]	98.20	NA	NA	NA
	CNN [20]	99.80	99	99	99
	ARM-Net [21]	97.11	96.87	96.66	97.77
	SNN	99.89	99.16	99.37	99.22
BraTS2021	CNN based Bayesian Optimized SVM [17]	97	96	96.6	96.6
	Relevance score with the AWA-based VGG-19 [18]	99.40	NA	NA	NA
	IGANN HBD-MI [19]	99.61	NA	98.5	97.2
	CNN [20]	99.29	99.78	99.3	99.15
	SNN	99.93	99.26	99.57	99.34

3.3 Discussion

Existing brain tumor segmentation and classification methods face several limitations. The CNN-based Bayesian Optimized SVM [17] suffers from high computational complexity due to its deep architecture, while the AWA-based VGG-19 model [18] is affected by vanishing gradient issues when handling complex datasets. Although IGANN HBD-MI [19] reduces overfitting, its performance is sensitive to noisy data. Conventional CNN [20] has limited ability to capture three-dimensional spatial relationships, and ARM-Net [21] may lose discriminative brain features, resulting in misclassification.

To overcome these challenges, the proposed SnnU-Net improves tumor boundary delineation through a sharpness-aware loss function, enabling accurate segmentation and effective feature extraction. The integrated feature extraction framework combines DWT, LTP, GLCM, HOG, shape, statistical, and histogram features to capture complementary frequency, texture, structural, and morphological information. Furthermore, the proposed Spiking Neural Network (SNN) with cognitive pruning eliminates redundant connections, reducing computational complexity while maintaining high classification accuracy. This combination enables efficient and robust brain tumor classification.

4. CONCLUSION

This research proposes a SNN for brain tumor classification due to its biologically inspired spiking neurons together with adaptive pruning mechanism helps remove unnecessary connections to decrease processing noise while maintaining better accuracy. The preprocessing step achieves MRI scan standardization through the normalization of image dimensions and intensity values. It leads to downstream task enhancement through the reduction of unpredictable factors while simultaneously optimizing tumor structure visibility. The introduction of standard dimensions in inputs accelerates both training process and inference operations. The SnnU-Net provides better boundaries at tumor delineations and accurate structural quality through its optimized skip connections together with advanced upsample processes. The feature extraction provides subsequent process to work effectively with better performance. The extracted features contain texture and shape with intensity-based characteristics that assist in tissue type discrimination. The proposed SNN achieves better

accuracy of 99.67%, 99.89% and 99.93% for BraTS2019, BraTS2020 and BraTS2021 datasets respectively. In future, metaheuristic algorithm based feature selection will be included to further enhance the classification performance.

REFERENCES

1. Celik, M. and Inik, O., 2024. Development of hybrid models based on deep learning and optimized machine learning algorithms for brain tumor Multi-Classification. Expert Systems with Applications, 238, p.122159.
2. Iqbal, S., Qureshi, A.N., Alhussein, M., Aurangzeb, K., Choudhry, I.A. and Anwar, M.S., 2024. Hybrid deep spatial and statistical feature fusion for accurate MRI brain tumor classification. Frontiers in Computational Neuroscience, 18, p.1423051.
3. Ullah, M.S., Khan, M.A., Almujally, N.A., Alhaisoni, M., Akram, T. and Shabaz, M., 2024. BrainNet: a fusion assisted novel optimal framework of residual blocks and stacked autoencoders for multimodal brain tumor classification. Scientific Reports, 14(1), p.5895.
4. Das, P. and Das, A., 2024. Multi-scale cross spectral coherence and phase spectral distribution based measurement in non-subsampled shearlet domain for classification of brain tumors. Expert Systems with Applications, 247, p.123329.
5. Kesav, O.H. and GK, R., 2024. Enhancing Brain Tumor Detection and Classification with Reduced Complexity Spatial Fusion Convolutional Neural Networks. International Journal of Intelligent Engineering & Systems, 17(1).
6. Pratap Joshi, K., Gowda, V.B., Bidare Divakarachari, P., Siddappa Parameshwarappa, P. and Patra, R.K., 2025. VSA-GCNN: Attention Guided Graph Neural Networks for Brain Tumor Segmentation and Classification. Big Data and Cognitive Computing, 9(2), p.29.
7. Dixit, A. and Thakur, M.K., 2025. 3W-MultiHier: A Three Way Multi-Hierarchical Model Enabled Deep Learning for Brain Tumor Classification in MRI Scans. Advanced Theory and Simulations, 8(3), p.2400752.
8. SenthilPandi, S., Senthilselvi, A., Kumaragurubaran, T. and Dhanasekaran, S., 2024. Self-attention-based generative adversarial network optimized with color harmony algorithm for brain tumor classification. Electromagnetic Biology and Medicine, pp.1-15.
9. Kavitha, P., Dhinakaran, D., Prabaharan, G. and Manigandan, M.D., 2024. Brain Tumor Detection for Efficient Adaptation and Superior Diagnostic Precision by Utilizing MBConv-Finetuned-B0 and Advanced Deep Learning. International Journal of Intelligent Engineering & Systems, 17(2).
10. Bhagyalaxmi, K. and Dwarakanath, B., 2025. CDCG-UNet: Chaotic Optimization Assisted Brain Tumor Segmentation Based on Dilated Channel Gate Attention U-Net Model. Neuroinformatics, 23(2), pp.1-26.
11. Kataria, J. and Panda, S.P., 2024. HybridCSF model for magnetic resonance image based brain tumor segmentation. Indonesian Journal of Electrical Engineering and Computer Science, 35(3), pp.1845-1852.
12. Sun, J., Hu, M., Wu, X., Tang, C., Lahza, H., Wang, S. and Zhang, Y., 2024. MVSI-Net: Multi-view attention and multi-scale feature interaction for brain tumor segmentation. Biomedical Signal Processing and Control, 95, p.106484.
13. AvazBeigi, M. and Ghazizadeh-Ahsaee, M., 2025. A Complete Preprocessing Pipeline for Brain Tumor Classification and Overall Survival Prediction Using Bidirectional Convolutional LSTM. SN Computer Science, 6(1), pp.1-13.
14. Dehghani, F., Karimian, A. and Arabi, H., 2024. Joint brain tumor segmentation from multi-magnetic resonance sequences through a deep convolutional neural network. Journal of Medical Signals & Sensors, 14(3), p.9.
15. Ahmad, J., Warraich, C.A.R., Ksibi, A., Alsenan, S., Arshad, A., Raza, R. and Shaikh, Z.A., 2025. LIU-NET: lightweight Inception U-Net for efficient brain tumor segmentation from multimodal 3D MRI images. PeerJ Computer Science, 11, p.e2787.
16. Yurtsever, M.E., Atay, Y., Arslan, B. and Sagiroglu, S., 2024. Development of brain tumor radiogenomic classification using GAN-based augmentation of MRI slices in the newly released gazi brains dataset. BMC Medical Informatics and Decision Making, 24(1), p.285.
17. Saeed, T., Khan, M.A., Hamza, A., Shabaz, M., Khan, W.Z., Alhayan, F., Jamel, L. and Baili, J., 2024. Neuro-XAI: Explainable deep learning framework based on deeplabV3+ and bayesian optimization for segmentation and classification of brain tumor in MRI scans. Journal of Neuroscience Methods, 410, p.110247.
18. Nancy, A.M. and Maheswari, R., 2025. Brain tumor segmentation and classification using transfer learning based CNN model with model agnostic concept interpretation. Multimedia Tools and Applications, 84(5), pp.2509-2538.
19. Kathirvel, N., Sasidhar, A., Rajasekaran, M. and Saravana Kumar, K., 2025. Optimized interpretable generalized additive neural network-based human brain diagnosis using medical imaging. Knowledge-Based Systems, 309, p.112862.
20. Bompem, G. and Pandluri, D., 2024. Batch Normalization Based Convolutional Neural Network for Segmentation and Classification of Brain Tumor MRI Images. International Journal of Intelligent Engineering & Systems, 17(2).
21. Dutta, T.K., Nayak, D.R. and Zhang, Y.D., 2024. Arm-net: Attention-guided residual multiscale cnn for multiclass brain tumor classification using mr images. Biomedical Signal Processing and Control, 87, p.105421.
22. BraTS2019 dataset link: https://www.kaggle.com/datasets/aryashah2k/brain-tumor-segmentation-brats-2019 (Accessed on April 2025).
23. BraTS2020 dataset link: https://www.kaggle.com/datasets/awsaf49/brats2020-training-data (Accessed on April 2025).
24. BraTS2021 dataset link: https://www.kaggle.com/datasets/dschettler8845/brats-2021-task1 (Accessed on April 2025).
25. Maaram, K.K. and Chandre, S., 2024. Feature Selection Using Adaptive Weber Distribution Based Flower Pollination Algorithm for Alzheimer's Disease Classification. SN Computer Science, 5(8), p.1085.